

Relaxation timescales and electron-phonon coupling in optically-pumped $\text{YBa}_2\text{Cu}_3\text{O}_{6+x}$ revealed by time-resolved Raman scattering.

N. Pellatz,^{1,2} S. Roy,^{1,2} J-W. Lee,³ J. L. Schad,³ H. Kandel,⁴ N. Arndt,⁴ C.B. Eom,³ and D. Reznik^{1,2,*}

¹*Department of Physics, University of Colorado, Boulder, Colorado 80309, USA*

²*Center for Experiments on Quantum Materials,
University of Colorado - Boulder, Boulder, Colorado, 80309, USA*

³*Department of Materials Science and Engineering,
University of Wisconsin-Madison, Madison, WI 53706, USA*

⁴*Department of Physics and Mathematics, University of Wisconsin-Parkside, Kenosha, WI 53140*

Quantum matter with striking properties has recently been generated by driving materials with ultrafast laser pulses. However, observing these phases by following a single property as a function of time after photoexcitation provides a limited picture. We directly tracked hot phonons and transient heating in a high temperature superconductor $\text{YBa}_2\text{Cu}_3\text{O}_{6.9}$ by time-resolved Raman scattering with time-resolution of 220 fs. In addition, we used the hardening of the Raman-active apical oxygen phonon right after photoexcitation as an indirect probe of hot electrons, which equilibrated with hot phonons around 0.5 ps. Analysis based on the two-temperature model revealed temperature-independent electron-phonon coupling with $\lambda \approx 0.8$ as well as significant anharmonicity that increased with temperature. It is essential to reduce this anharmonicity to generate longer lived nonequilibrium states in copper oxides. We also discuss new insights into photoinduced superconductivity recently reported at lower doping that follow from these results.

Driving quantum materials with electromagnetic fields can generate novel phases and states away from thermal equilibrium [1–5]. Recently reported signatures of superconductivity at elevated temperatures in photoexcited copper oxides and intercalated fullerenes are particularly interesting but still enigmatic [6–12]. In most of these experiments the ultrafast laser pulse (pump) drives or photoexcites the system and another ultrafast pulse (probe) takes snapshots of a specific property as a function of pump-probe time delay. For example infrared (IR) reflectivity probes the optical response, and x-ray diffraction is sensitive to the crystal structure. Such experiments also elucidate energy flows between phonons, electrons, and magnons providing a way to determine the strength of different interactions.

This work focuses on relaxation timescales and interactions between electrons and phonons in a prototypical copper oxide superconductor, $\text{YBa}_2\text{Cu}_3\text{O}_{6.9}$.

Electron-phonon coupling in the copper oxides is still enigmatic. It allows electron-hole recombination with the creation of phonons, and phonons in turn can decay into electron-hole pairs. As a result, spectroscopic quasiparticle peaks shift and/or broaden due to decreased lifetime. However phonon-phonon coupling (anharmonicity) also broadens the phonon peaks and electron-electron interactions can broaden the electronic quasiparticles. Disorder can further increase the linewidths [13], so extracting electron-phonon coupling strength from the linewidths of quasiparticle peaks is challenging.

We used time-resolved Raman scattering (TRR) to get around this problem following earlier work [14–21]. In TRR an ultrafast pump laser pulse first photoexcites the material and Raman scattering from another

time-delayed pulse probes the system. Its built-in time resolution is perfect for investigating short-lived optically pumped phases. In the copper oxides, previous TRR work highlighted ultrafast destruction of the antiferromagnetic order in the undoped parent compound of $\text{YBa}_2\text{Cu}_3\text{O}_{6+x}$ [22] and nonequilibrium behavior of the superconducting gap in $\text{Bi}_2\text{Sr}_2\text{CaCu}_2\text{O}_{8+\delta}$ (BSCCO) [23].

In our experiment near IR pump pulses created hot electrons, and the time-delayed Raman probe measured occupation number and energy of the apical oxygen A_{1g} phonon (Fig. 1b) known for a large spectroscopic linewidth [24–26] and an anomaly at the superconducting transition temperature, T_c . Apical oxygen modes recently came to the center of attention due to their impact on electronic [27] and magnetic [28] degrees of freedom of the copper-oxygen planes, interlayer charge transport [29], and photoinduced superconductivity [6, 9–11, 27].

The experiment demonstrated strong electron-phonon coupling of this phonon, i.e. it is one of the hot phonons of the two-temperature model confirming previous theoretical results [30–35]. Initial dramatic increase of its occupation number was followed by thermalization with electrons and other hot phonons. Subsequent relaxation due to anharmonic decay of hot phonons into other phonons was significantly faster than in graphite [15–21] and its rate increased from base temperature to room temperature (Fig. 1b). Electron-phonon interaction was temperature-independent within uncertainty and its strength λ was ≈ 0.8 (Fig. 1b).

The investigated sample was a 170 nm-thick (110)-oriented $\text{YBa}_2\text{Cu}_3\text{O}_{6.9}$ thin film prepared by pulsed laser deposition on a (110) LaAlO_3 substrate with T_c of 81 K [36, 37]. Our TRR setup (Fig. 1c) uses 20 kHz 790 nm (1.57 eV) laser pulses from an amplified mode-locked Ti:sapphire laser which produces intense 40 fs pulses.

* Corresponding Author: dmitry.reznik@colorado.edu

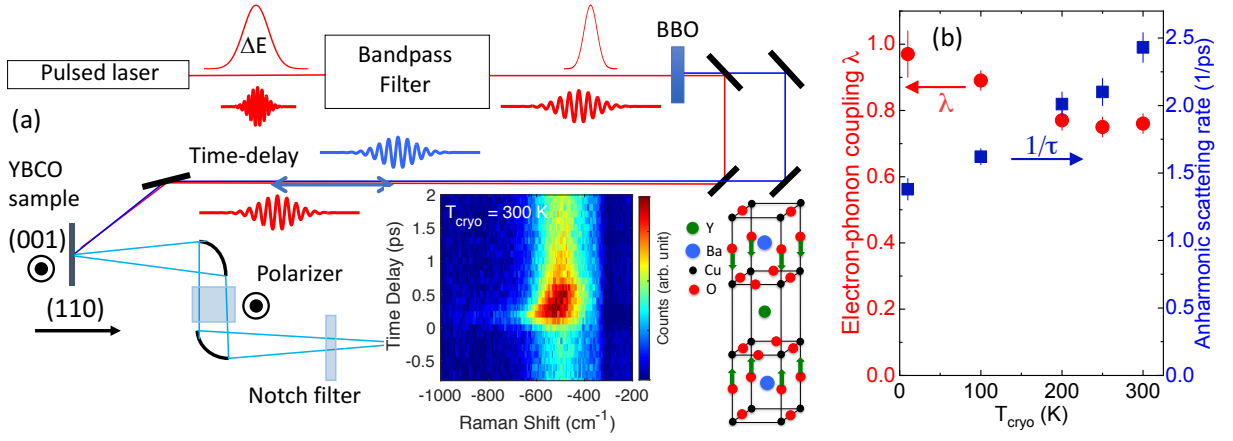


FIG. 1. Time-resolved Raman scattering (TRR) setup and key results. (a) Schematic of the TRR experiment and the color map showing representative data on the anti-Stokes (AS) side of the spectrum obtained with the sample at 300 K. Negative time corresponds to the probe pulse arriving before the pump pulse when the system is still at thermal equilibrium. Most intensity in the peak is from the Raman-active apical oxygen phonon whose atomic displacements are indicated by green arrows in the schematic of the $\text{YBa}_2\text{Cu}_3\text{O}_7$ unit cell to the right of the color map. Note the dramatic increase in intensity and shift to a larger energy at small delay times. (b) Electron-phonon coupling constant λ together with the anharmonic scattering rate $1/\tau$. See Supplementary Notes 2 and 3 for details on how τ and λ were calculated.

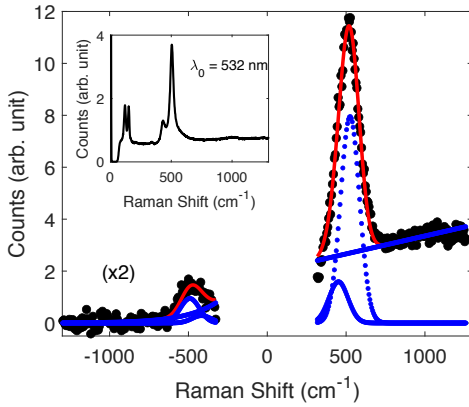


FIG. 2. Fits to the raw data for the sample at 300 K and $t = -1000$ fs. Stokes side: the fit is to two gaussian peaks at 440 and 500 cm^{-1} plus a linear background. The anti-Stokes side was fit to the same peaks and background multiplied by the ratio given in Eq. (1). Inset: data taken with the 532 nm CW laser, showing the two phonons at 440 and 500 cm^{-1} .

Second harmonic generation at 395 nm (3.14 eV) was used as the probe light source for Raman scattering.

The time-energy uncertainty principle limits the energy resolution of the ultrafast probe. In the standard high time-resolution configuration the probe pulse is too broad in energy so that its tails wash out the apical oxygen phonon peak at 500 cm^{-1} . In order to get around this problem the 790 nm pulses were passed through an in-house built time-compensating band-pass filter before the second harmonic generation making both the pump and the probe pulses narrower in energy and broader in time. A cross-correlation measurement gave a time-resolution of 220 fs FWHM (see Supplementary Note 1).

The time-averaged probe power was kept below 1 mW, which eliminated self-pumping nonlinearities [17].

The scattered light was collected by a pair of parabolic mirrors with a polarizer in the middle, and analyzed on a single-stage McPherson spectrometer equipped with a LN_2 -cooled CCD detector. A custom-made notch filter blocked elastically-scattered light. All measurements were done either in air, at room temperature, or in a cryostat in a He exchange gas. We show results obtained with the pump photon polarization parallel to the ab-plane. Photon polarization along the c-axis gave similar results. Background measured under identical conditions but without the probe was subtracted from raw data.

We read off phonon temperature from the intensities on the Stokes (S) and anti-Stokes (AS) sides, I_S and I_{AS} [15, 16]. They are related by the fundamental principle of detailed balance:

$$\frac{gI_{AS}}{I_S} = \frac{(\omega_0 + \omega_{ph})^4}{(\omega_0 - \omega_{ph})^4} e^{-\hbar\omega_{ph}/k_B T_{ph}}, \quad (1)$$

where ω_0 is the laser frequency, ω_{ph} is the phonon energy, k_B is the Boltzmann's constant, T_{ph} is the phonon temperature, and g is equal to 1. To correct for systematic error, we made $g = 0.9$, chosen to make the phonon temperature at negative times equal to 300 K at room temperature. Following convention, we define the temperature of each bosonic mode, T_{boson} , via its relation to the occupation number $n = (e^{\hbar\omega_{ph}/k_B T_{boson}} - 1)^{-1}$. Away from thermal equilibrium different phonons have different occupation numbers, and therefore different temperatures. According to the fluctuation-dissipation theorem, the S and AS Raman intensities are given by $I_S = (n + 1)\chi''(\hbar\omega)$, and $I_{AS} = n\chi''(\hbar\omega)$, where χ'' is the imaginary part of the Raman response function

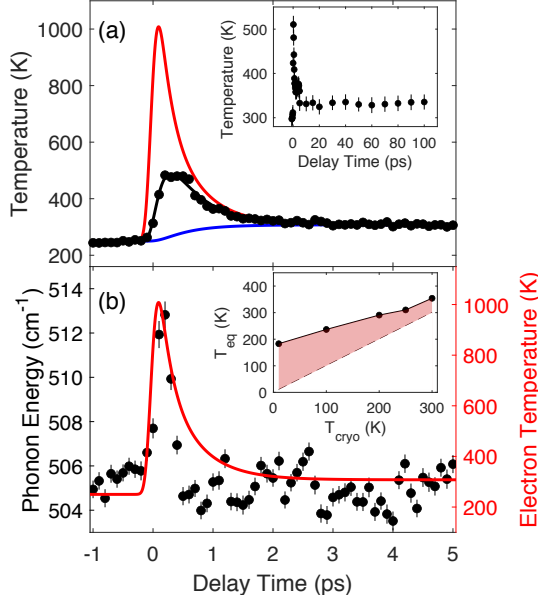


FIG. 3. Phonon temperature and energy at the temperature in the cryostat $T_{cryo} = 250$ K together with fits to two temperature model as described in the text. Pump (probe) fluence was 1.4 mJ/cm^2 ($15 \text{ } \mu\text{J/cm}^2$). Black line represents hot phonons, red – hot electrons, blue – cold phonons. The electronic temperature curves in (a) (b) are the same. Inset to (a) illustrates the behavior at large delay times for the sample in air at 300 K. Inset to (b) shows the temperature at which internal thermalization occurs, T_{eq} , as a function of T_{cryo} . The difference between the dashed line and the data in the inset to (b) represents transient heating ΔT .

(polarizability) of the phonon of interest.

The color map in Fig. 1a showcases the dramatic increase of the AS intensity as well as a peak shift to larger energy observed right after photoexcitation. This result implies a significant increase of the phonon temperature right after the arrival of the pump pulse (Eqs. 1,2).

The apical oxygen phonon around 500 cm^{-1} (inset to Fig. 1b) and a weaker plane oxygen mode at 440 cm^{-1} dominate the Raman spectrum in the zz geometry where both incident and scattered photons are polarized perpendicular to the copper-oxygen planes (Fig. 2) [24, 25, 38]. When fitting the time-resolved data where the peaks are not resolved (Fig. 2 main panel), the intensity of the 440 cm^{-1} peak was fixed at 20% of the 500 cm^{-1} peak, consistent with Raman intensities obtained with a high energy resolution 360 nm laser whose wavelength is close to 395 nm of the probe pulsed laser. The linewidths of the two peaks are similar (Fig. 2 inset), so we assumed similar electron-phonon coupling and kept the intensity ratio the same at all delay times. Assuming weak electron-phonon coupling for the 440 cm^{-1} peak did not significantly change the fit results.

The phonon temperature dramatically increases within the time-resolution to about 450 K independent of the temperature in the cryostat (Fig. 3a). This increase is followed by the exponential decay starting from 0.5 ps with ~ 478 fs lifetime at $T_{cryo} = 250$ K. The decay satu-

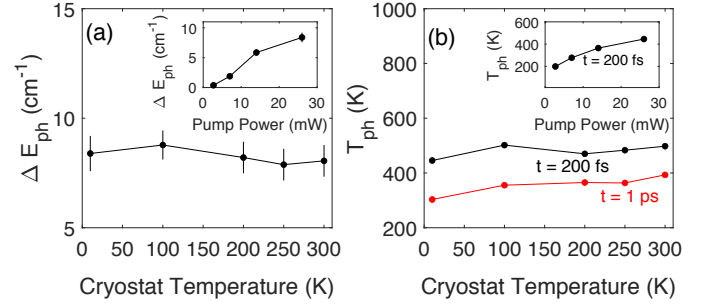


FIG. 4. Dependence on pump power, P , and T_{cryo} . (a) Phonon hardening at 200 fs ($E_{ph}(200 \text{ fs}) - E_{ph}(-1000 \text{ fs})$) as a function of T_{cryo} at $P = 27 \text{ mW}$. Inset: Phonon hardening at $T_{cryo} = 10$ K as a function of P . (b) Phonon temperature at 200 fs and 1 ps as a function of T_{cryo} at $P = 27 \text{ mW}$ (fluence of 1.4 mJ/cm^2). Note that $T_{el} = T_{ph}$ at 1 ps. Inset: T_{ph} at 200 fs at $T_{cryo} = 10$ K as a function of P .

rates around 5 ps (Fig. 3a inset) when the photoexcited region reaches the internal thermal equilibrium temperature, $T_{eq} = 300$ K. Inset to Fig. 2b shows T_{eq} as a function of T_{cryo} highlighting increased transient heating of the sample, ΔT , at lower temperatures due to its smaller heat capacity. ΔT reaches 170 K at $T_{cryo} = 10$ K. Further equilibration with the cryostat exchange gas is much longer than 100 ps, which is much slower than the timescales relevant here (see inset to Fig. 3a).

Our pump photon energy of 1.5 eV is far from resonance with any phonons. Instead pump photons should create electron-hole pairs [39], which thermalize among themselves much faster than the time resolution. Thus effectively the pump pulse rapidly heats electrons to a high temperature. Time resolved angle-resolved photoemission (trARPES) showed that electrons reached a maximum temperature of 800 K with $100 \text{ } \mu\text{J/cm}^2$ pump pulses in BSCCO [40]. In graphite the electronic temperature reached far above 1000 K when pumping with $150 \text{ } \mu\text{J/cm}^2$ [15, 41, 42]. It is reasonable to expect similarly high electronic temperatures in YBCO right after photoexcitation in our experiments.

We argue that it is possible to qualitatively deduce the electronic temperature from the shift of the phonon peak position to a higher energy (hardening) at small time delays (Fig. 3c). The hardening at 200 fs is independent of temperature in the cryostat but decreases with reduced pump power (Fig. 4a). Consider a phonon softened by strong electron-phonon coupling at room temperature and below. Heating of electrons will smear the Fermi surface, which will reduce the softening, i.e. phonon hardening will occur [43]. A similar effect in graphite was associated with electronic temperatures of over 1000 K [17]. So the phonon hardening at short delay times indicates electronic temperatures far above 500 K.

We interpret our results in terms of the two-temperature model where f is a fraction of phonons with strong electron-phonon coupling, λ . Photoexcited electrons first give off energy to the hot phonons [40, 44, 45], which in turn decay into other, cold phonons with the

lifetime τ until all phonons and electrons thermalize at T_{eq} . The system then slowly equilibrates with the heat bath via propagating (mostly acoustic) phonons. Our experiments provide detailed information on each step of this process.

The electrons are pumped by a Gaussian pulse $P(t)$ with energy density $E_{pulse} = c_{tot}\Delta T$, where $\Delta T = T_{eq} - T_{cryo}$ and duration of 170 fs. The combined specific heat of electrons, hot phonons, and cold phonons, c_{tot} , depends on temperature, but we approximate it as the average of the values at T_{cryo} and T_{eq} . If Ω_0 is a typical phonon energy, then the electronic temperature, T_{el} , the hot phonon temperature, T_h , and the cold phonon temperature, T_c , obey the rate equations

$$\frac{\partial T_{el}}{\partial t} = -\frac{3\lambda\Omega_0^3}{\hbar\pi k_B} \frac{n(T_{el}) - n(T_h)}{T_{el}} + \frac{P(t)}{c_{el}(T_{el})}, \quad (2)$$

$$\frac{\partial T_h}{\partial t} = \frac{c_{el}(T_{el})}{c_h(T_h)} \frac{3\lambda\Omega_0^3}{\hbar\pi k_B} \frac{n(T_{el}) - n(T_h)}{T_{el}} - \frac{T_h - T_c}{\tau}, \quad (3)$$

$$\frac{\partial T_c}{\partial t} = \frac{c_h(T_h)}{c_c(T_c)} \frac{T_h - T_c}{\tau}, \quad (4)$$

where $n(T) = (e^{\Omega_0/k_B T} - 1)^{-1}$ and the specific heats are $c_{el} = \gamma T_{el}$, $c_h = 3N_{atm}f\Omega_0(\partial n_h/\partial T_h)$, and $c_c = 3N_{atm}(1-f)\Omega_0(\partial n_c/\partial T_c)$. Here, N_{atm} is the number of atoms per formula unit ($= 12.9$ for our sample) and the value of γ was taken from measurements in Ref. [46]. Equations 2-4 correspond to equations 1-3 of Ref. [40] written down in terms of ΔT , which we measured with high precision.

We solved these coupled differential equations using the Euler method with 1 fs steps. Fig. 3a presents a fit to this model with $\Omega_0 = 60$ meV and $\tau = 478$ fs (see Supplementary Note 3 for fits with different values of Ω_0 and τ). $f = 0.14$ and $\lambda = 0.75$ were free parameters. The fixed parameters match the time-dependence of T_{el} to phonon hardening in Fig. 3b and T_{ph} to the temperature dependence of the phonon occupation numbers in Fig. 3a. Electrons initially heat up to 1000 K similarly to the previous result on BSCCO [40], and then cool quickly to thermalize with hot phonons at 300 fs. Thermalized hot electrons and hot phonons have a larger heat capacity compared with the heat capacity of electrons alone so they equilibrate with cold phonons with the much slower 478 fs time constant at 250 K. This lifetime increases at low temperatures reaching 700 fs at 10 K (see Supplementary Note 2 and Fig. 1b). The electron-phonon coupling strength is close to $\lambda = 0.8$ at all temperatures, which is similar to λ extracted from the two-magnon scattering spectrum of insulating YBCO [47]. It is more than double the LDA value [48], presumably due to the overestimate of screening by LDA [30, 31].

After the discovery of superconductivity in the cuprates, the initial assessment that electron-phonon

coupling in cuprates was weak [49] was followed by discoveries of strong electron-phonon coupling of select zone center phonons [24–26, 50]. Subsequent inelastic neutron and x-ray scattering experiments revealed an even stronger coupling of plane oxygen bond-stretching and bond-buckling branches around half-way between the zone center and the zone boundary [51, 52], and theory highlighted strong electron-phonon coupling of several modes [30–32]. Our experiment demonstrated a similarly strong electron-phonon coupling of the zone center apical oxygen phonon. Its role in the pairing interaction depends on the wavevector-dependence of electron-phonon coupling thus it is imperative to investigate this phonon away from the zone center.

Our work provides new insights into photoinduced superconductivity whose signatures were reported in the optical spectra of underdoped YBCO when pumping with the photons resonating with IR-active c-axis apical oxygen vibration and with the same 790 nm near-IR pulses as in our experiments [9]. We found that these optical features correspond to the time-delays at which hot and cold phonons are out of thermal equilibrium, but electrons and hot phonons are at or near thermal equilibrium. Photoinduced superconductivity may occur in electrons at or above room temperature under the second pumping scenario with the caveat that there may be significant differences between optimally-doped YBCO and underdoped YBCO where photoinduced superconductivity was reported. We also demonstrated strong electron-phonon coupling of the Raman active counterpart of the IR-active phonons, where apical oxygens vibrate along the c-axis with a different relative phase. Lineshape changes of the IR mode consistent with electron-phonon coupling were also reported [53]. Pumping this phonon would heat electrons due to its decay into electron-hole pairs [29–31]. It is necessary to determine if this heating is large or small. Photoinduced superconductivity disappears close to the time-delays at which anharmonicity-driven thermalization occurs, so reducing anharmonicity should extend the lifetime of the photoinduced state.

To conclude, we used time-resolved Raman scattering to investigate a high quality nearly-optimally-doped YBCO thin film. Pumping electrons with 790 nm ultrafast laser pulses boosted Raman-active apical oxygen phonon occupation numbers relative to other phonons rapidly and dramatically, proving its strong electron-phonon coupling. Rapid thermalization due to strong anharmonicity limits the lifetime of nonequilibrium phases in YBCO. Electron-phonon coupling was stronger than expected from LDA and nearly temperature independent between 10 K and 300 K, whereas the anharmonicity increased significantly between low temperatures and room temperature. The electrons were heated far above room temperature throughout the time delays and cryostat temperatures at which superconductivity induced by the near IR pump has been reported at lower oxygen concentrations [54, 55].

- [1] Y. H. Wang, H. Steinberg, P. Jarillo-Herrero, and N. Gedik, Observation of floquet-bloch states on the surface of a topological insulator, *Science* **342**, 453 (2013), <https://science.sciencemag.org/content/342/6157/453.full.pdf>.
- [2] A. Kirilyuk, A. V. Kimel, and T. Rasing, Ultrafast optical manipulation of magnetic order, *Rev. Mod. Phys.* **82**, 2731 (2010).
- [3] P. Tengdin, W. You, C. Chen, X. Shi, D. Zusin, Y. Zhang, C. Gentry, A. Blonsky, M. Keller, P. M. Oppeneer, *et al.*, Critical behavior within 20 fs drives the out-of-equilibrium laser-induced magnetic phase transition in nickel, *Science Advances* **4**, 9744 (2018).
- [4] H. Okamoto, T. Miyagoe, K. Kobayashi, H. Uemura, H. Nishioka, H. Matsuzaki, A. Sawa, and Y. Tokura, Photoinduced transition from mott insulator to metal in the undoped cuprates Nd_2CuO_4 and La_2CuO_4 , *Phys. Rev. B* **83**, 125102 (2011).
- [5] H. Ehrke, R. Tobey, S. Wall, S. Cavill, M. Först, V. Khanna, T. Garl, N. Stojanovic, D. Prabhakaran, A. Boothroyd, *et al.*, Photoinduced melting of antiferromagnetic order in $\text{LaO}_{0.5}\text{Sr}_{1.5}\text{MnO}_4$ measured using ultrafast resonant soft x-ray diffraction, *Phys. Rev. Lett.* **106**, 217401 (2011).
- [6] W. Hu, S. Kaiser, D. Nicoletti, C. R. Hunt, I. Gierz, M. C. Hoffmann, M. Le Tacon, T. Loew, B. Keimer, and A. Cavalleri, *Optically Enhanced Coherent Transport in $\text{YBa}_2\text{Cu}_3\text{O}_{6.5}$ by Ultrafast Redistribution of Interlayer Coupling*, *Nature Materials* **13**, 705 (2014).
- [7] M. Mitrano, A. Cantaluppi, D. Nicoletti, S. Kaiser, A. Perucchi, S. Lupi, P. Di Pietro, D. Pontiroli, M. Riccò, S. R. Clark, D. Jaksch, and A. Cavalleri, *Possible Light-Induced Superconductivity in K_3C_{60} at High Temperature*, *Nature* **530**, 461 (2016).
- [8] M. Budden, T. Gebert, M. Buzzi, G. Jotzu, E. Wang, T. Matsuyama, G. Meier, Y. Laplace, D. Pontiroli, M. Riccò, F. Schlawin, D. Jaksch, and A. Cavalleri, *Evidence for Metastable Photo-Induced Superconductivity in K_3C_{60}* (2020), arXiv:2002.12835 [cond-mat.supr-con].
- [9] B. Liu, M. Först, M. Fechner, D. Nicoletti, J. Porras, T. Loew, B. Keimer, and A. Cavalleri, *Pump Frequency Resonances for Light-Induced Incipient Superconductivity in $\text{YBa}_2\text{Cu}_3\text{O}_{6.5}$* , *Physical Review X* **10**, 10.1103/physrevx.10.011053 (2020).
- [10] D. Nicoletti, E. Casandruc, Y. Laplace, V. Khanna, C. R. Hunt, S. Kaiser, S. S. Dhesi, G. D. Gu, J. P. Hill, and A. Cavalleri, *Optically Induced Superconductivity in Striped $\text{La}_{2-x}\text{Ba}_x\text{CuO}_4$ by Polarization-Selective Excitation in the Near Infrared*, *Phys. Rev. B* **90**, 100503 (2014).
- [11] K. A. Cremin, J. Zhang, C. C. Homes, G. D. Gu, Z. Sun, M. M. Fogler, A. J. Millis, D. N. Basov, and R. D. Averitt, *Photoenhanced Metastable c -axis Electrodynamics in Stripe-Ordered Cuprate $\text{La}_{1.885}\text{Ba}_{0.115}\text{CuO}_4$* , *Proceedings of the National Academy of Sciences* **116**, 19875 (2019).
- [12] Y. Takabayashi and K. Prassides, *Unconventional high- T_c Superconductivity in Fullerides*, *Philosophical Transactions of the Royal Society A: Mathematical, Physical and Engineering Sciences* **374**, 20150320 (2016).
- [13] S. R. Park, A. Hamann, L. Pintschovius, D. Lamago, G. Khaliullin, M. Fujita, K. Yamada, G. D. Gu, J. M. Tranquada, and D. Reznik, *Effects of Charge Inhomogeneities on Elementary Excitations in $\text{La}_{2-x}\text{Sr}_x\text{CuO}_4$* , *Phys. Rev. B* **84**, 214516 (2011).
- [14] D. von der Linde, J. Kuhl, and H. Klingenberg, Raman scattering from nonequilibrium lo phonons with picosecond resolution, *Phys. Rev. Lett.* **44**, 1505 (1980).
- [15] J.-A. Yang, S. Parham, D. Dessau, and D. Reznik, *Novel Electron-Phonon Relaxation Pathway in Graphite Revealed by Time-Resolved Raman Scattering and Angle-Resolved Photoemission Spectroscopy*, *Scientific Reports* **7**, 40876 (2017).
- [16] J. A. Kash, J. C. Tsang, and J. M. Hvam, *Subpicosecond Time-Resolved Raman Spectroscopy of LO Phonons in GaAs*, *Phys. Rev. Lett.* **54**, 2151 (1985).
- [17] H. Yan, D. Song, K. F. Mak, I. Chatzakis, J. Maultzsch, and T. F. Heinz, *Time-Resolved Raman Spectroscopy of Optical Phonons in Graphite: Phonon Anharmonic Coupling and Anomalous Stiffening*, *Phys. Rev. B* **80**, 121403 (2009).
- [18] D. Song, F. Wang, G. Dukovic, M. Zheng, E. D. Semke, L. E. Brus, and T. F. Heinz, *Direct Measurement of the Lifetime of Optical Phonons in Single-Walled Carbon Nanotubes*, *Phys. Rev. Lett.* **100**, 225503 (2008).
- [19] K. Kang, T. Ozel, D. G. Cahill, and M. Shim, *Optical Phonon Lifetimes in Single-Walled Carbon Nanotubes by Time-Resolved Raman Scattering*, *Nano letters* **8**, 4642 (2008).
- [20] K. Kang, D. Abdula, D. G. Cahill, and M. Shim, *Lifetimes of Optical Phonons in Graphene and Graphite by Time-Resolved Incoherent anti-Stokes Raman Scattering*, *Phys. Rev. B* **81**, 165405 (2010).
- [21] S. Wu, W.-T. Liu, X. Liang, P. J. Schuck, F. Wang, Y. R. Shen, and M. Salmeron, *Hot Phonon Dynamics in Graphene*, *Nano letters* **12**, 5495 (2012).
- [22] J.-A. Yang, N. Pellatz, T. Wolf, R. Nandkishore, and D. Reznik, *Ultrafast Magnetic Dynamics in Insulating $\text{YBa}_2\text{Cu}_3\text{O}_{6.1}$ Revealed by Time Resolved Two-Magnon Raman Scattering*, *Nature Communications* **11**, 2548 (2020).
- [23] R. P. Saichu, I. Mahns, A. Goos, S. Binder, P. May, S. G. Singer, B. Schulz, A. Rusydi, J. Unterhinninghofen, D. Manske, P. Guptasarma, M. S. Williamsen, and M. Rübhausen, *Two-Component Dynamics of the Order Parameter of High Temperature $\text{Bi}_2\text{Sr}_2\text{CaCu}_2\text{O}_{8+\delta}$ Superconductors Revealed by Time-Resolved Raman Scattering*, *Phys. Rev. Lett.* **102**, 177004 (2009).
- [24] M. F. Limonov, A. I. Rykov, S. Tajima, and A. Yamanaka, *Raman Scattering in $\text{YBa}_2\text{Cu}_3\text{O}_7$ Single Crystals: Anisotropy in Normal and Superconductivity States*, *Physics of the Solid State* **40**, 367 (1998).
- [25] E. Altendorf, J. Chrzanowski, J. C. Irwin, A. O'Reilly, and W. N. Hardy, *Electron-Phonon Interactions of Raman Active Phonons in $\text{YBa}_2\text{Cu}_3\text{O}_{7-y}$* , *Physica C: Superconductivity* **175**, 47 (1991).
- [26] K. F. McCarty, H. B. Radousky, J. Z. Liu, and R. N. Shelton, *Temperature Dependence of the Linewidths of the Raman-Active Phonons of $\text{YBa}_2\text{Cu}_3\text{O}_7$: Evidence for a Superconducting Gap Between 440 and 500 cm^{-1}* , *Phys. Rev. B* **43**, 13751 (1991).
- [27] B. Rosenstein and B. Y. Shapiro, *Apical Oxygen Vibrations Dominant Role in Cuprate Superconductivity and its Interplay with Spin Fluctuations* (2020),

- arXiv:2003.03521 [cond-mat.supr-con].
- [28] Y. Y. Peng, G. Dellea, M. Minola, M. Conni, A. Amorese, D. Di Castro, G. M. De Luca, K. Kummer, M. Saluzzo, X. Sun, X. J. Zhou, G. Balestrino, M. Le Tacon, B. Keimer, L. Braicovich, N. B. Brookes, and G. Ghiringhelli, Influence of apical oxygen on the extent of in-plane exchange interaction in cuprate superconductors, *Nature Physics* **13**, 1201 (2017).
 - [29] M. H. Michael, A. von Hoegen, M. Fechner, M. Först, A. Cavalleri, and E. Demler, Parametric resonance of josephson plasma waves: A theory for optically amplified interlayer superconductivity in $\text{YBa}_2\text{Cu}_3\text{O}_{6+x}$ (2020), arXiv:2004.13049 [cond-mat.supr-con].
 - [30] O. Gunnarsson and O. Rösch, Interplay between electron-phonon and coulomb interactions in cuprates, *Journal of Physics: Condensed Matter* **20**, 043201 (2008).
 - [31] S. Johnston, F. Vernay, B. Moritz, Z.-X. Shen, N. Nagaosa, J. Zaanen, and T. P. Devereaux, Systematic study of electron-phonon coupling to oxygen modes across the cuprates, *Phys. Rev. B* **82**, 064513 (2010).
 - [32] A. Alexandrov and P. Kornilovitch, High-temperature superconductivity and charge segregation in a model with strong long-range electron-phonon and coulomb interactions, *Physics Letters A* **299**, 650 (2002).
 - [33] C. Falter, M. Klenner, and G. A. Hoffmann, Phonon renormalization and c-axis phonon-plasmon mixing in La_2CuO_4 , *Phys. Rev. B* **52**, 3702 (1995).
 - [34] C. Falter, M. Klenner, and W. Ludwig, Effect of charge fluctuations on the phonon dispersion and electron-phonon interaction in La_2CuO_4 , *Phys. Rev. B* **47**, 5390 (1993).
 - [35] O. Rösch, O. Gunnarsson, X. J. Zhou, T. Yoshida, T. Sasagawa, A. Fujimori, Z. Hussain, Z.-X. Shen, and S. Uchida, Polaronic behavior of undoped high- T_c cuprate superconductors from angle-resolved photoemission spectra, *Phys. Rev. Lett.* **95**, 227002 (2005).
 - [36] J. Z. Wu, P. Y. Hsieh, A. V. McGuire, D. L. Schmidt, L. T. Wood, Y. Shen, and W. K. Chu, *Anisotropic Properties of the High-Quality Epitaxial $\text{YBa}_2\text{Cu}_3\text{O}_{7-\delta}$ (110) Thin Film*, *Phys. Rev. B* **44**, 12643 (1991).
 - [37] M. S. Raven, E. E. Inameti, S. Iwama, Y. M. Wan, and B. G. Murray, *Epitaxial Growth and Critical Currents in (013)/(103)- and (110)-oriented $\text{YBa}_2\text{Cu}_3\text{O}_x$ Films*, *Phys. Rev. B* **52**, 6845 (1995).
 - [38] D. Reznik, M. V. Klein, W. C. Lee, D. M. Ginsberg, and S.-W. Cheong, *Effect of Conduction Electrons on the Polarized Raman Spectra of Copper Oxide Superconductors*, *Phys. Rev. B* **46**, 11725 (1992).
 - [39] S. L. Cooper, D. Reznik, A. Kotz, M. A. Karlow, R. Liu, M. V. Klein, W. C. Lee, J. Giapintzakis, D. M. Ginsberg, B. W. Veal, and A. P. Paulikas, *Optical Studies of the a-, b-, and c-axis Charge Dynamics in $\text{YBa}_2\text{Cu}_3\text{O}_{6+x}$* , *Phys. Rev. B* **47**, 8233 (1993).
 - [40] L. Perfetti, P. A. Loukakos, M. Lisowski, U. Bovensiepen, H. Eisaki, and M. Wolf, *Ultrafast Electron Relaxation in Superconducting $\text{Bi}_2\text{Sr}_2\text{CaCu}_2\text{O}_{8+\delta}$ by Time-Resolved Photoelectron Spectroscopy*, *Phys. Rev. Lett.* **99**, 197001 (2007).
 - [41] Y. Ishida, T. Togashi, K. Yamamoto, M. Tanaka, T. Taniuchi, T. Kiss, M. Nakajima, T. Suemoto, and S. Shin, *Non-Thermal Hot Electrons Ultrafastly Generating Hot Optical Phonons in Graphite*, *Scientific reports* **1**, 64 (2011).
 - [42] M. Breusing, C. Ropers, and T. Elsaesser, *Ultrafast Carrier Dynamics in Graphite*, *Phys. Rev. Lett.* **102**, 086809 (2009).
 - [43] D. Lamago, M. Hoesch, M. Krisch, R. Heid, K.-P. Bohnen, P. Böni, and D. Reznik, Measurement of strong phonon softening in cr with and without fermi-surface nesting by inelastic x-ray scattering, *Phys. Rev. B* **82**, 195121 (2010).
 - [44] J. C. Johannsen, S. Ulstrup, F. Cilento, A. Crepaldi, M. Zacchigna, C. Cacho, I. C. E. Turcu, E. Springate, F. Fromm, C. Roidel, T. Seyller, F. Parmigiani, M. Griioni, and P. Hofmann, *Direct View of Hot Carrier Dynamics in Graphene*, *Phys. Rev. Lett.* **111**, 027403 (2013).
 - [45] T. Kampftrath, L. Perfetti, F. Schapper, C. Frischkorn, and M. Wolf, *Strongly Coupled Optical Phonons in the Ultrafast Dynamics of the Electronic Energy and Current Relaxation in Graphite*, *Phys. Rev. Lett.* **95**, 187403 (2005).
 - [46] J. W. Loram, K. A. Mirza, J. R. Cooper, and W. Y. Liang, Electronic specific heat of $\text{yba}_2\text{cu}_3\text{o}_{6+x}$ from 1.8 to 300 k, *Phys. Rev. Lett.* **71**, 1740 (1993).
 - [47] D. Farina, G. De Filippis, A. S. Mishchenko, N. Nagaosa, J.-A. Yang, D. Reznik, T. Wolf, and V. Cataudella, Electron-phonon coupling in the undoped cuprate $\text{yba}_2\text{cu}_3\text{o}_6$ estimated from raman and optical conductivity spectra, *Phys. Rev. B* **98**, 121104 (2018).
 - [48] K.-P. Bohnen, R. Heid, and M. Krauss, Phonon dispersion and electron-phonon interaction for $\text{yba}_2\text{cu}_3\text{o}_7$ from first-principles calculations, *Europhysics Letters (EPL)* **64**, 104 (2003).
 - [49] S. Y. Savrasov and O. K. Andersen, Linear-response calculation of the electron-phonon coupling in doped cacuo_2 , *Phys. Rev. Lett.* **77**, 4430 (1996).
 - [50] L. Pintschovius, Electron-phonon coupling effects explored by inelastic neutron scattering, *physica status solidi (b)* **242**, 30 (2005), <https://onlinelibrary.wiley.com/doi/pdf/10.1002/pssb.200404951>.
 - [51] D. Reznik, *Phonon Anomalies and Dynamic Stripes*, *Physica C: Superconductivity* **481**, 75 (2012).
 - [52] M. Raichle, D. Reznik, D. Lamago, R. Heid, Y. Li, M. Bakr, C. Ulrich, V. Hinkov, K. Hradil, C. T. Lin, and B. Keimer, *Highly Anisotropic Anomaly in the Dispersion of the Copper-Oxygen Bond-Bending Phonon in Superconducting $\text{YBa}_2\text{Cu}_3\text{O}_7$ from Inelastic Neutron Scattering*, *Phys. Rev. Lett.* **107**, 177004 (2011).
 - [53] A. Pashkin, M. Porer, M. Beyer, K. W. Kim, A. Dubroka, C. Bernhard, X. Yao, Y. Dagan, R. Hackl, A. Erb, J. Demsar, R. Huber, and A. Leitenstorfer, Femtosecond response of quasiparticles and phonons in superconducting $\text{YBa}_2\text{Cu}_3\text{O}_{7-\delta}$ studied by wideband terahertz spectroscopy, *Phys. Rev. Lett.* **105**, 067001 (2010).
 - [54] C. R. Hunt, D. Nicoletti, S. Kaiser, D. Pröpper, T. Loew, J. Porras, B. Keimer, and A. Cavalleri, *Dynamical Decoherence of the Light Induced Interlayer Coupling in $\text{YBa}_2\text{Cu}_3\text{O}_{6+\delta}$* , *Phys. Rev. B* **94**, 224303 (2016).
 - [55] S. Kaiser, C. R. Hunt, D. Nicoletti, W. Hu, I. Gierz, H. Y. Liu, M. Le Tacon, T. Loew, D. Haug, B. Keimer, and A. Cavalleri, *Optically Induced Coherent Transport far above T_c in underdoped $\text{YBa}_2\text{Cu}_3\text{O}_{6+\delta}$* , *Phys. Rev. B* **89**, 184516 (2014).

I. ACKNOWLEDGEMENTS

We would like to thank A. Cavalleri for a critical reading of the manuscript and helpful suggestions. Experiments at the University of Colorado were supported by the NSF under Grant No. DMR-1709946 and laboratory upgrade that made these experiments possible by DARPA through the DRINQS program. The work

at University of Wisconsin-Madison (thin film synthesis and structural and electrical characterizations) was supported by the US Department of Energy (DOE), Office of Science, Office of Basic Energy Sciences (BES), under award number DE-FG02-06ER46327. The work at the University of Wisconsin-Parkside was supported by WiSys and UW System Applied Research Grant award number 102-4-812000-AAH1775.